Hindawi
Journal of Nanomaterials
Volume 2022, Article ID 2680489, 13 pages
https://doi.org/10.1155/2022/2680489

Research Article

Analytical Assessment of MHD Flow of Nanoliquid Subject to Thermal Radiation and Brownian Effect

Haroon Ur Rasheed,[1] **Ebenezer Bonyah**,[2] **Soumaya Gouadria**,[3] **Waris Khan**,[4] **Ahmed Alshehri**,[5] **and Raees Khan**[6]

[1]*Department of Computer Science, Sarhad University of Science and Information Technology Peshawar, 25000 KP, Pakistan*
[2]*Department of Mathematics Education, Akenten Appiah Menka University of Skills Training and Entrepreneurial Development, (Kumasi Campus), Ghana*
[3]*Department of Physics, College of Science, Princess Nourah bint Abdulrahman University, P.O. Box 84428, Riyadh 11671, Saudi Arabia*
[4]*Department of Mathematics and Statistics, Hazara University Mansehra, 21120 KP, Pakistan*
[5]*Department of Mathematics, Faculty of Science, King Abdulaziz University, Jeddah 21589, Saudi Arabia*
[6]*Department of Mathematics, FATA University, Darra Adam Khel, FR Kohat, 26300 KP, Pakistan*

Correspondence should be addressed to Ebenezer Bonyah; ebbonya@gmail.com

Received 19 October 2021; Accepted 28 March 2022; Published 28 April 2022

Academic Editor: Domenico Acierno

This manuscript studies the impact of the heat and mass flow and chemical reaction with electromagnetic field and heat flow of non-Newtonian Walter-B nanofluid via the uniform magnetic field. A mathematical model is used to simulate the arisen nonlinear partial differential equations (PDEs). By employing the suitable transformations, the system of PDEs is then transformed to a nonlinear system of ordinary differential equations (ODEs). The impact of the pertinent parameters on the velocity profile, energy, and concentration distribution has been discussed. These nonlinear coupled equations were addressed analytically by implementing an efficient and validated analytical method, where Mathematica 11.0 programming code is established for simulating the flow system. Stability and convergence analysis have been performed in order to improve the accuracy of the flow system. In order to gain physical insight, the effects of dimensionless parameters on flow fields are investigated. In addition, the impression of system parameters on skin-friction, heat transfer coefficient, and mass flow rate profiles is also debated.

1. Introduction

Nanomaterials have been of great interest to engineers as well as to scientists during the previous decades. As a matter of fact, nanomaterials are known to enhance the thermal conductivity of base fluids. The first one who suggested the addition of carbon nanotubes and solid particles in base fluids was Maxwell [1]. The results achieved were motivational; however, some problems were raised such as pressure drop enhancement and pipe erosion. Then, Choi et al. [2] proposed the notion of carbon nanotubes and nanoscaled particles in base fluids and named them as nanofluids. Metals, such as Ag and Cu, and metal oxides, such as Al_2O_3 and CuO, are the most widely used nanoparticles. Improved nanofluids' thermal conductivity has important applications not only in domestic heating but also in heat exchangers and cooling systems. Nanofluids, discovered by Choi [3], are colloids composed of nanoparticles and base fluid. Nanoparticles have thermal conductivity, typically greater in magnitude than base fluids and significantly smaller in size than 100 nm. The work of nanoparticles greatly improves the heat transfer efficiency of the base fluids. Basic fluids can be water, synthetic liquids, fats, lubricants and blood. Nanoparticles are synthetic materials with

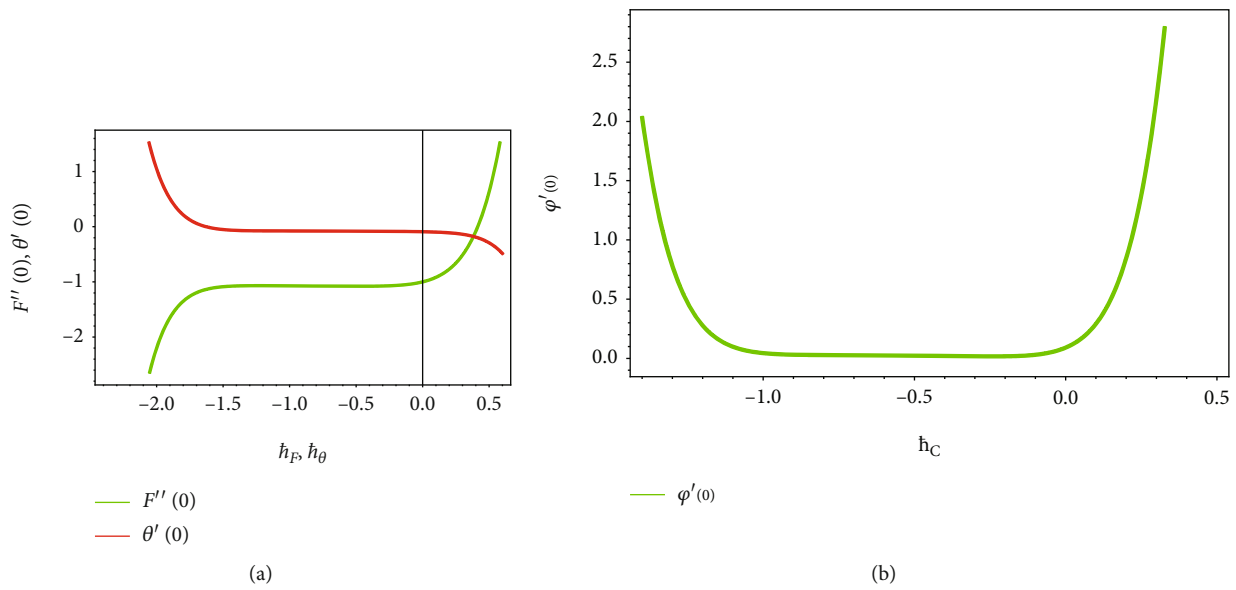

FIGURE 1: (a) $\hbar$ – *curves* for $F(\varsigma)$ and $\theta(\varsigma)$ functions. (b) $\hbar$ – *curves* for $\varphi(\varsigma)$ function.

substantial use in biomedicine because of the special manner in which they interact with matter. Hybrid nanofluids are a particular type of nanofluid. Hybrid nanofluids are formed by the suspension in the base fluid of two or more kinds of nanoparticles with hybrid nanoparticles. Hybrid nanoparticle is a specific substance that integrates the physical and chemical characteristics of different materials at the same time and has been commonly used in the production of antitumor medicines. Some studies that discuss nanofluids and hybrid nanofluids are reported in the refs. [4–10]. Magnetic fluid flow due to the rotating body has potential applications in biomedical sciences, electronic devices, and aerodynamics [11]. Hafeez et al. investigated the flow of an Oldroyd-B fluid type's magnetic fluid in a rotating system using modified Fourier's law [12]. Reddy et al. reported the influence of hybrid nanoparticles in a swirling flow using an activation energy model [13]. Fluid flow investigation in biomicrofluidic systems is implemented by the electroosmosis process. The latter is the principal instrument for the stream activation in a wide scope of utilization. This electroosmotic transition takes place in such a way that, as long as the polar outer layer is connected to the electrolyte device, the counterparts of the electrolyte should be allowed to pass through the surface of the capacitor and ultimately to build a membrane with a high convergence of counteractors, which is commonly named after the Stern layer. In addition to the exterior diffuse coat, the Electric Double Layer (EDL) is produced in the area of the charged board. Applying the ambient electrical field to the electroosmotic flow (EOF), the functional particles in the dispersed area of the EOF are induced to travel and accomplish fluid displacement, which is typically known as the "EOF." Propelled by the monumental use of the stream of the electroassimilation, various experiments are investigated [14–18]. Christopher et al. [19] discussed the chemical reaction consequence on the flow of hybrid nanoliquid on an SS with Cattaneo–Christov heat flux. Gowda et al. [20] examined the convective stream of second grade fluid on a coiled SS with Dufour and Soret effects. Alhadhrami et al. [21] pondered the LTNE impact on the flow of Casson liquid on an SS with a porous medium. Recently, Ali et al. [22–26] conferred the flow of different fluid past stretching surfaces with several influencing factors by considering different nanoparticles' suspension. Another significant nonmechanical micropump is the electromagnetohydrodynamic (EMHD) which has different applications, some of which, fluid mixing and pumping along with flow control in microfluidic systems [27–29]. Lorentz force is generated because of an electric field force applied across the channel in the presence of a perpendicular magnetic field force. Reddy et al. reported the influence of hybrid nanoparticles in a swirling flow using an activation energy model [13]. Khan demonstrated the transportation of hybrid nanoparticles in convective flow due to a rotating plate [30]. Hayat et al. considered the viscous dissipation and Joule heating in the flow due to a rotating plate with variable thickness [31]. The following references [32–37] provide more about thermal radiation and activation energy.

TABLE 1: The allowable ranges for convergence solutions.

Approximate solutions	Auxiliary parameters	Convergent intervals
$F(\varsigma)$	$\hbar_F$	$-1.4 \le \hbar_F \le -0.4$
$\theta(\varsigma)$	$\hbar_\theta$	$-1.2 \le \hbar_\theta \le -0.5$
$\varphi(\varsigma)$	$\hbar_\varphi$	$-0.7 \le \hbar_\varphi \le -0.3$

In this study, we explored the nature of stagnation point flow of nanoliquid driven by stretching surface. The role of Brownian motion and thermophoresis is also considered in modeling the flow system. The mechanisms of heat and

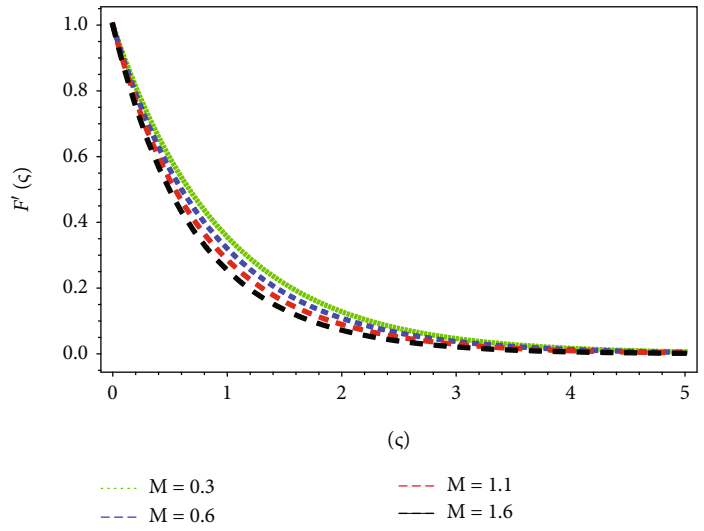

Figure 2: Plot of $F'(\varsigma)$ via diverse M.

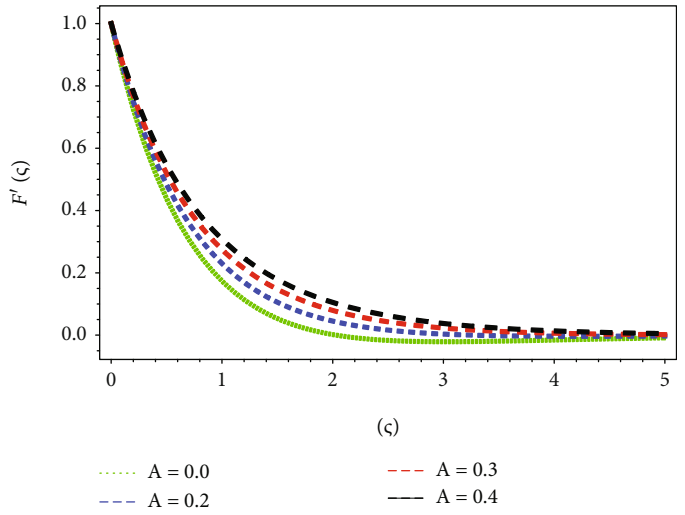

Figure 3: Plot of $F'(\varsigma)$ via diverse A.

mass flow are also are examined. The arisen nonlinear partial differential equations are altered to ODEs via transformations and then solved analytically [38–40]. Following are the key points of this investigation:

(i) The main goal of this study is to examine the two-dimensional incompressible Walters-B nanofluid flow over a stretching sheet. Furthermore, the graphs are also used to discuss the variations in detailed profiles as a consequence of several dimensionless parameters

(ii) To study time subservient Walter-B fluid flow resulting from the impression of heat and mass transfer

(iii) Mathematical modeling of the fundamental flow equations comprises momentum, energy, and diffusion balances

2. Problem Formulation

Consider the magnetohydrodynamic MHD flow of a Walter-B non-Newtonian nanofluid with heat transfer transient through a two-dimensional conduit. The impact of Brownian and thermophoretic effects is considered into the account. Additionally, the thermal radiation, Joule heating, viscous dissipation, and heat generation/absorption characteristics are taken into consideration. The fluid is electrically conductive in nature along with uniform magnetic field B_0 in normal direction. Based on these assumptions with the approximations of the boundary layer, the basic equations of Walter-B fluid reduced as follow [31]:

$$\frac{\partial \bar{u}}{\partial \bar{x}} + \frac{\partial \bar{v}}{\partial \bar{y}} = 0, \tag{1}$$

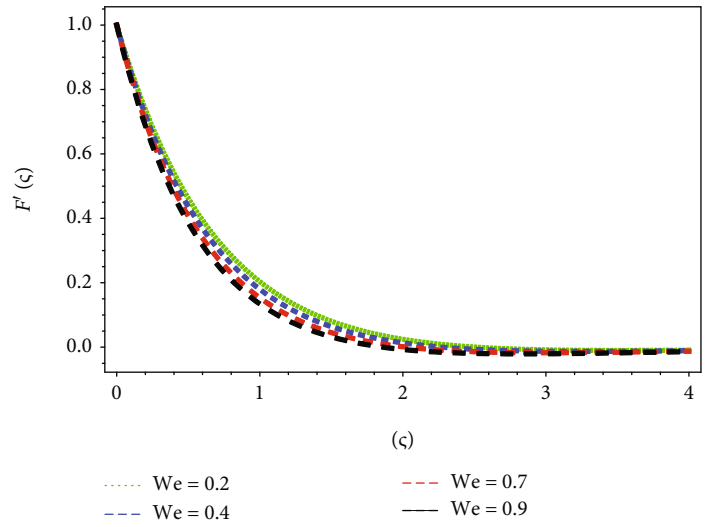

Figure 4: Plot of $F'(\varsigma)$ via diverse We.

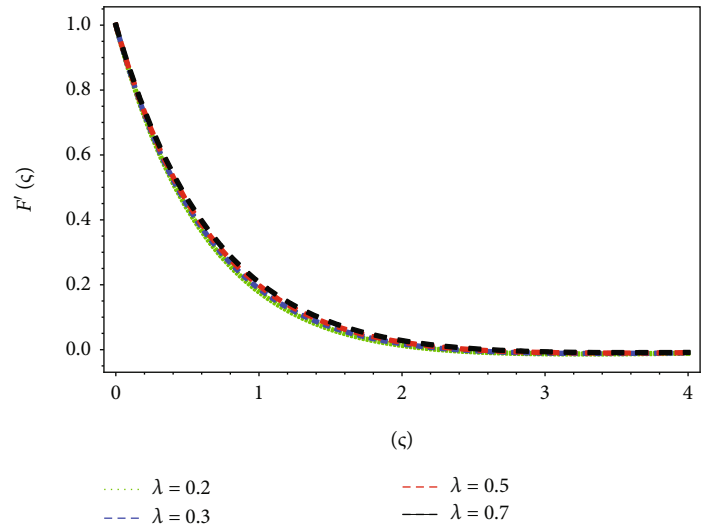

Figure 5: Plot of $F'(\varsigma)$ via diverse λ.

$$\bar{u}\frac{\partial \bar{u}}{\partial \bar{x}} + \bar{v}\frac{\partial \bar{u}}{\partial \bar{y}} = u_e\frac{\partial u_e}{\partial \bar{x}} + \nu\frac{\partial^2 \bar{u}}{\partial(\bar{y})^2} - \frac{k_0}{\rho_f}\left(\bar{u}\frac{\partial^3 \bar{u}}{\partial \bar{x}\partial(\bar{y})^2} + \bar{v}\frac{\partial^3 \bar{u}}{\partial(\bar{y})^3} + \frac{\partial \bar{u}}{\partial \bar{x}}\frac{\partial^2 \bar{u}}{\partial(\bar{y})^2} - \frac{\partial \bar{u}}{\partial \bar{y}}\frac{\partial^2 \bar{u}}{\partial \bar{x}\partial \bar{y}}\right) + \frac{\sigma B_0^2}{\rho_f}(u_e - \bar{u}) + g\beta_T(\bar{T} - \bar{T}_\infty) - g\beta_C(\bar{C} - \bar{C}_\infty), \tag{2}$$

$$\bar{u}\frac{\partial \bar{T}}{\partial \bar{x}} + \bar{v}\frac{\partial \bar{T}}{\partial \bar{y}} = \alpha\frac{\partial^2 \bar{T}}{\partial \bar{y}^2} - \frac{1}{(\rho c)_f}\frac{16\sigma^*}{3k^*}\frac{\partial}{\partial \bar{y}}\left(\bar{T}^3\frac{\partial \bar{T}}{\partial \bar{y}}\right) + \frac{\sigma B_0^2 \bar{u}^2}{(\rho c)_f} + \tau\left[D_B\frac{\partial \bar{C}}{\partial \bar{y}}\frac{\partial \bar{T}}{\partial \bar{y}} + \frac{D_T}{\bar{T}_\infty}\left(\frac{\partial \bar{T}}{\partial \bar{y}}\right)^2\right] + \frac{Q_0}{(\rho c)_f}(\bar{T} - \bar{T}_\infty), \tag{3}$$

$$\bar{u}\frac{\partial \bar{C}}{\partial \bar{x}} + v^*\frac{\partial \bar{C}}{\partial \bar{y}} = D_B\left(\frac{\partial^2 \bar{C}}{\partial(\bar{y})^2}\right) + \frac{D_T}{\bar{T}_\infty}\left(\frac{\partial^2 \bar{T}}{\partial(\bar{y})^2}\right) - k_r^2 e^{-E_a/kT^*}\left(\frac{\bar{T}}{\bar{T}_\infty}\right)^m(\bar{C} - \bar{C}_\infty), \tag{4}$$

with boundary postulates [31]

$$\bar{u} = u_w(\bar{x}) = c_1\bar{x}, v = 0, -k\frac{\partial \bar{T}}{\partial \bar{y}} = (\bar{T}_s - \bar{T})h_1, -D_B\frac{\partial \bar{C}}{\partial \bar{y}} = (\bar{C}_s - \bar{C})h_2 : \bar{y} = 0$$
$$\bar{u} = u_e = c_2\bar{x}, \bar{T} \longrightarrow \bar{T}_\infty, \bar{C} \longrightarrow \bar{C}_\infty : \bar{y} \longrightarrow \infty, \tag{5}$$

whereas $(\bar{u}, \bar{v})$ are velocity component in $\bar{x}-$ and $\bar{y}-$ *direction*, u_e is the free stream velocity, D_B Brownian motion, D_T thermophoretic coefficient, g gravitational acceleration, $\bar{C}$ fluid concentration, $\bar{T}$ temperature; $\alpha = k/\rho c_f$ thermal

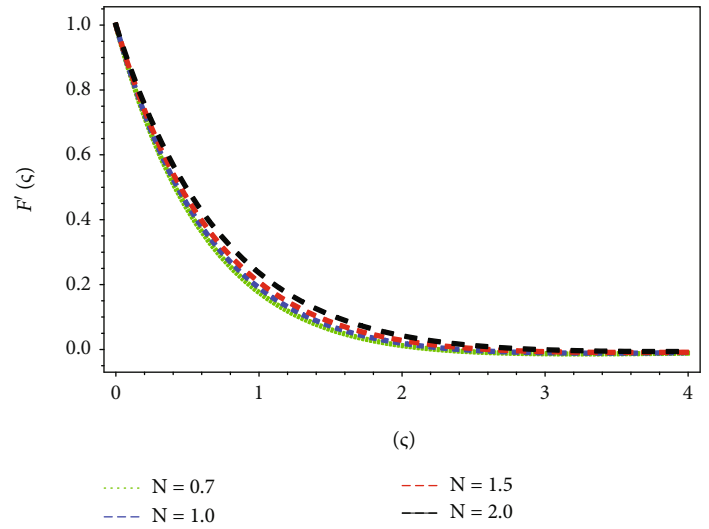

Figure 6: Plot of $F'(\varsigma)$ via diverse N.

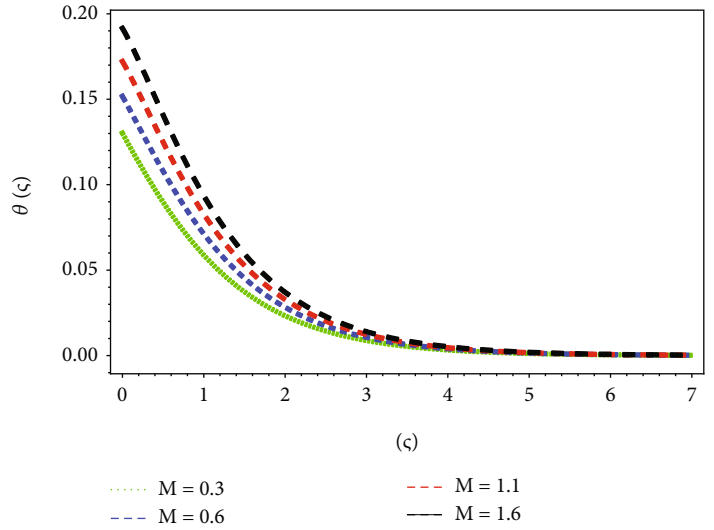

Figure 7: Impact of M on temperature field.

diffusion coefficient, $\nu = \mu_0/\rho_f$ kinematic viscosity, σ^* is the Stefan-Boltzmann constant, k^* absorption coefficient, $\beta_{\bar{C}}$ denote the solutal expansion coefficient, $\beta_{\bar{T}}$ thermal expansion coefficient, τ heat capacity ratio, σ electrical conductivity, Q_0 heat generation/absorption, Ea activation energy, $\bar{T}_s$ surface temperature, $\bar{C}_s$surface concentration, h_1 heat transfer coefficient, h_2 mass transfer coefficient, m fitted rate constant, kr reaction rate, $\bar{T}_\infty$ ambient temperature, $\bar{C}_\infty$ ambient concentration, and k_0 short memory coefficient.

Adopting the local transformation similarity [31]:

$$\bar{u} = c_1 \bar{x} F'(\varsigma), \bar{v} = -(c_1\nu)^{1/2} F(\varsigma), \varsigma = \sqrt{\frac{c_1}{\nu}}\bar{y}, \theta = \frac{\bar{T} - \bar{T}_\infty}{\bar{T}_s - \bar{T}_\infty}, \varphi = \frac{\bar{C} - \bar{C}_\infty}{\bar{C}_s - \bar{C}_\infty}, \tag{6}$$

After incorporating Equation (6), one gets the dimensional Equations (2)–(5) into dimensionless form:

$$F''' - F'2 + FF'' + \mathrm{We}\left(F''2 - 2F'F''' + FF''''\right) + M\left(A - F'\right) + A^2 + \lambda(\theta + N\varphi) = 0, \tag{7}$$

$$\left(\left(1 + \frac{3}{4}R\left(1 + \left(\theta_f - 1\right)\theta\right)^3\right)\theta'\right)' + \mathrm{Pr}\left(F\theta' + Nb\theta'\varphi' + Nt\theta'2 + MEcF'^2 + S\theta\right) = 0, \tag{8}$$

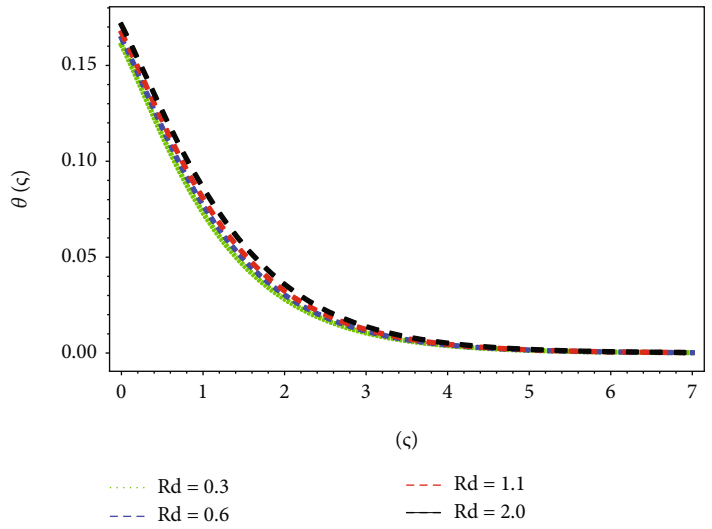

Figure 8: Impact of R on temperature field.

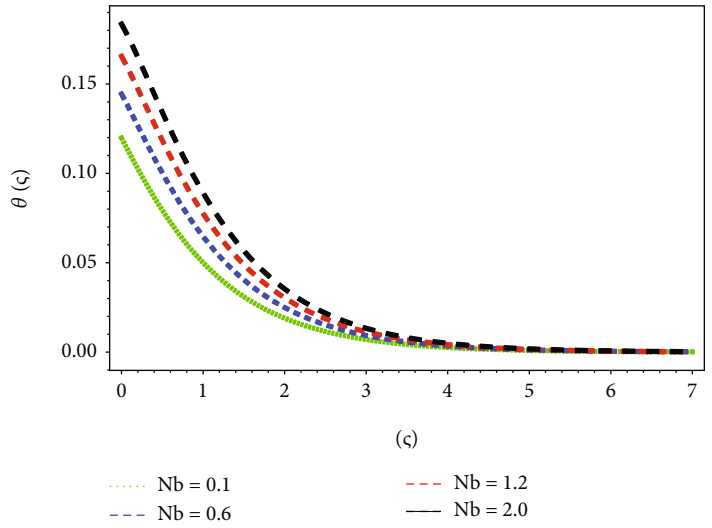

Figure 9: Impact of Nb on temperature field.

$$\varphi'' + ScF\varphi' + \left(\frac{Nt}{Nb}\right)\theta'' - Sc\sigma(1+\delta_1\theta)^m\varphi \exp\left[\frac{-E_1}{1+\delta_1\theta}\right] = 0, \tag{9}$$

$$\begin{aligned} &F = 0, F' = 1, \theta' = -\alpha(1-\theta), \varphi' = -\beta(1-\varphi): \\ &\varsigma = 0 \text{ and } F' = A, \theta = 0, \varphi = 0 : \varsigma = \infty \end{aligned} \tag{10}$$

where $We = k_0 c_1/\mu_0$ is the Weissenberg number, $\lambda = g\beta_{\bar{T}}/c_1^2\,\bar{x}(\bar{T}_s - \bar{T}_\infty)$ mixed convection parameter, $M = \sigma B_0^2/\rho_f c_1$ magnetic parameter, $N = g\beta_{\bar{C}}/c_1^2\bar{x}(\bar{C}_s - \bar{C}_\infty)$ ratio of thermal to concentration buoyancy forces, $Nt = \tau D_T/T_\infty^* \nu(\bar{T}_s - \bar{T}_\infty)$ thermophoresis force, $Nb = \tau D_B/\nu(\bar{C}_s - \bar{C}_\infty)$ Brownian motion, $\delta_1 = \bar{T}_s - \bar{T}_\infty/\bar{T}_\infty$ temperature difference, $R = 4\sigma^*(\overline{T_\infty})^3/kk^*$ radiation factor, $S = Q_0/(\rho c)_f c_1$ heat generation factor, $Ec = \bar{u}_w^2/c_f(\bar{T}_s - \bar{T}_\infty)$ Eckert number, $B_1 = h_1/k\sqrt{\nu/y}$ thermal Biot number, $B_2 = h_2/D_B\sqrt{\nu/y}$ Biot number, $\Pr = \mu c_p/k$ Prandtl number, $Sc = \nu/D_B$ Schmidt number, $\sigma = k_r^2/c_1$ dimensionless reaction rate, $A = c_2/c_1$ ratio of constants, $\theta_F = \bar{T}_w/\bar{T}_\infty$ temperature ratio parameter, and $E_1 = E_a/\kappa\bar{T}_\infty$ activation energy.

The physical quantities for the engineering practical and usefulness are the local skin friction, temperature gradient, and concentration gradient. The dimensionless form of these quantities is, respectively, expressed as follows

$$\sqrt{\mathrm{Re}_x}Cf_x = \left(1 - 3B\frac{dF}{d\varsigma}\frac{d^2F}{d\varsigma^2}\right)_{\varsigma=0}, \tag{11}$$

$$\frac{Nu_x}{\sqrt{\mathrm{Re}_x}} = -\left(1 + \frac{4}{3}R\left(1 + \left(T_f - 1\right)T\right)^3\right)\left.\frac{d\theta}{d\varsigma}\right|_{\varsigma=0}, \tag{12}$$

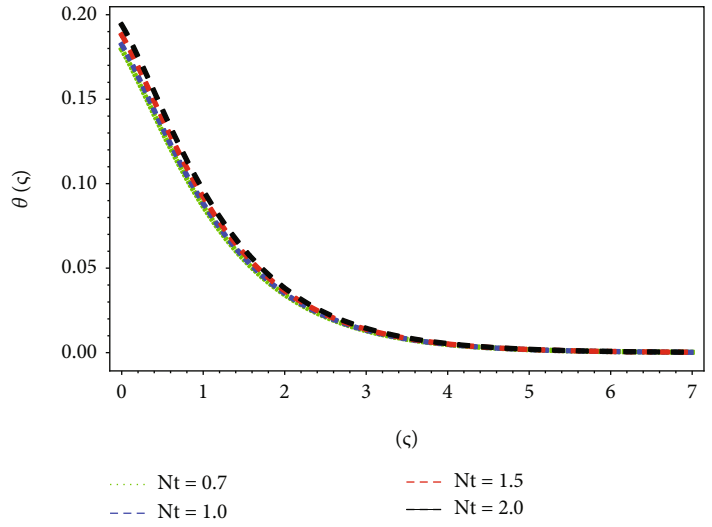

Figure 10: Impact of Nt on temperature field.

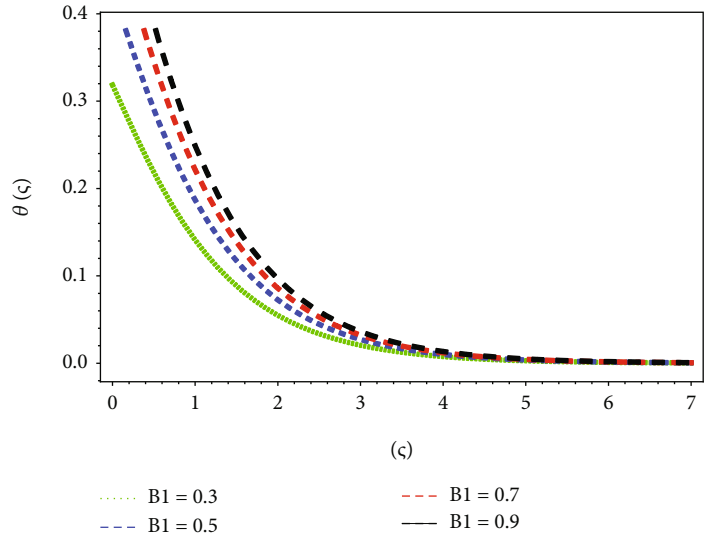

Figure 11: Impact of B_1 on temperature field.

One can obtain the Cf_x in nondimensional form by substituting Equation (12) in Equation (12):

$$\frac{Sh_x}{\sqrt{\mathrm{Re}_x}} = -\frac{d\varphi}{d\varsigma}\bigg|_{\varsigma=0}, \tag{13}$$

$\mathrm{Re}_x = c_1 x^2/\nu$ is the local Reynold number.

3. Convergence and Stability Analysis

The series solutions developed by the homotopic analysis method (HAM) comprise the convergence control parameters $\hbar_F, \hbar_\theta$ and $\hbar_\varphi$ [36–38]. These convergence control parameters are effective at regulating and controlling the series solution convergence region. The admissible values are attained by the flat parts of the $\hbar-curves$. Figure 1 displays the acceptable ranges of $\hbar_F, \hbar_\theta$ and $\hbar_\varphi$ are $-1.4 \le \hbar_F \le -0.4$, $-1.2 \le \hbar_\theta \le -0.5$ and $-0.7 \le \hbar_\varphi \le -0.3$. Table 1 display the convergence region for the approximate solutions.

4. Discussions

This section discusses the graphical implications of the physical dimensionless quantities on the relevant profiles. By selecting appropriate similarity variables, the equations that reflect the specified flow are converted first into ODEs. To clearly understand the behavior of flow profiles, an analytical scheme is adopted, which is strategized and debated using graphs.

Figure 2 portrays the sway of M on velocity $F'(\varsigma)$ portraits of stagnation point flow of nanofluids. It is noticed that velocity distributions diminish with higher values of magnetic parameter M. In reality, the fluid viscosity increases as M apply to any fluid due to which magnetic field power

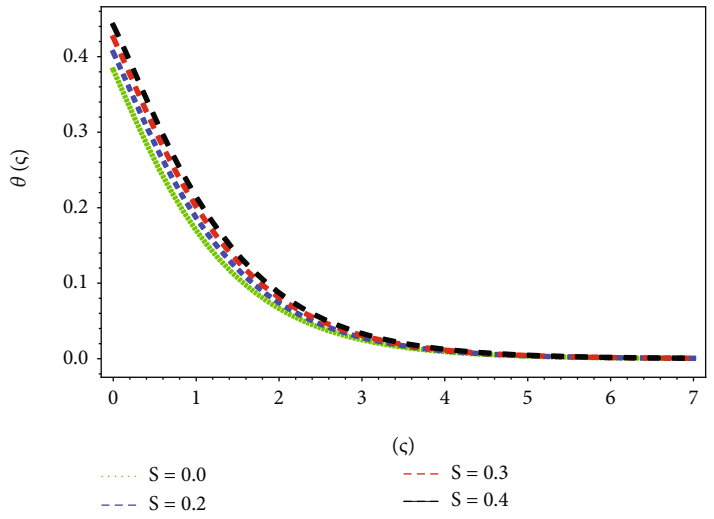

Figure 12: Impact of S on temperature field.

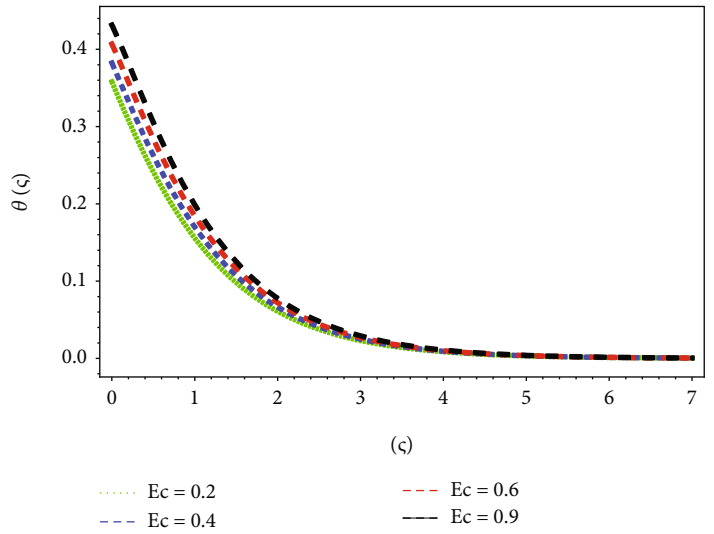

Figure 13: Impact of Ec on temperature field.

increase. In consequences, Lorentz force is produced which slows down the fluid flow significantly. It is observed from Figure 3 that the velocity sketches are enhance in the entire flow domain of nanofluid with the increasing values of ratio parameter A. Figure 4 reveals the sway of Weissenberg number We on velocity sketches of stagnation point flow of nanofluid. It is pointed out that in the intensification in $F'(\varsigma)$ field with step up values ofWenumber. The sketches of velocity fields with augmented values of mixed convection parameter λ in the flow domain are illustrated through Figure 5. This is owing to the fact that the increasing values of λ increase the buoyancy force. Consequently, $F'(\varsigma)$ profiles increase. It is detected from Figure 6 that the $F'(\varsigma)$ profiles of the nanofluid intensify in the fluid region with higher estimation of ratio of thermal to concentration buoyancy forces N.

The distribution of $\theta(\varsigma)$ temperature of nanofluid with step up values of M is presented in Figure 7. It is observed that boundary layer thickness improves with incrementing values of M. This is due to the fact that Lorentz force which acts against the fluid flow direction, hence the enhancement in $\theta(\varsigma)$ profiles with increasing values of M in the entire fluid flow. Attributes' features of radiation parameter R on $\theta(\varsigma)$ are exposed in Figure 8. It is perceived from this plot that the $\theta(\varsigma)$ sketches enhance in the entire flow of nanofluid with increasing data of R. The sketches of $\theta(\varsigma)$ field with augmented values of Nb in the flow region are describes through Figure 9. The energy sketches are enlarged with increasing data of Nb. This owes due to the motion of nanoparticles in the base fluid that is influenced by the motion of particles, and it moves from hot surface region and is related to the size and agglomeration of molecules. It is observed in Figure 10 that $\theta(\varsigma)$ intensify subject to increasing value of Nt parameter. In reality, the thermophoretic forces and the nanoscale solid particles in the base liquid produce warm surfaces in the boundary layer region. Thus, $\theta(\varsigma)$ of nanofluid in the entire fluid flow boosts. The effect of thermal

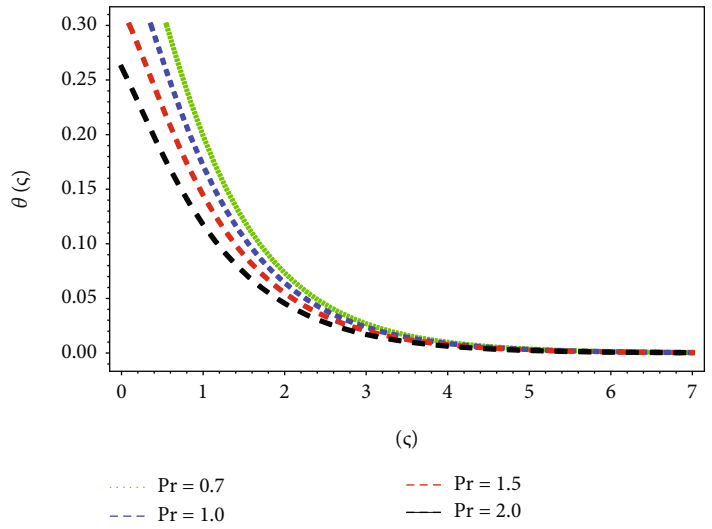

Figure 14: Impact of Pr on temperature field.

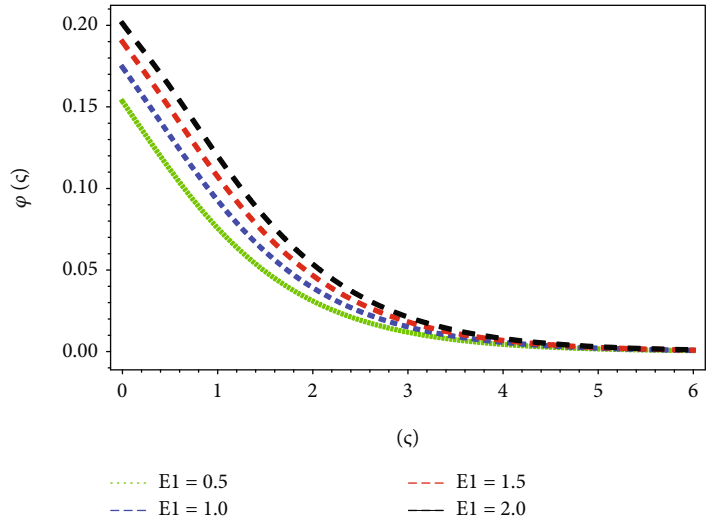

Figure 15: Nanoparticle volume fraction via E_1.

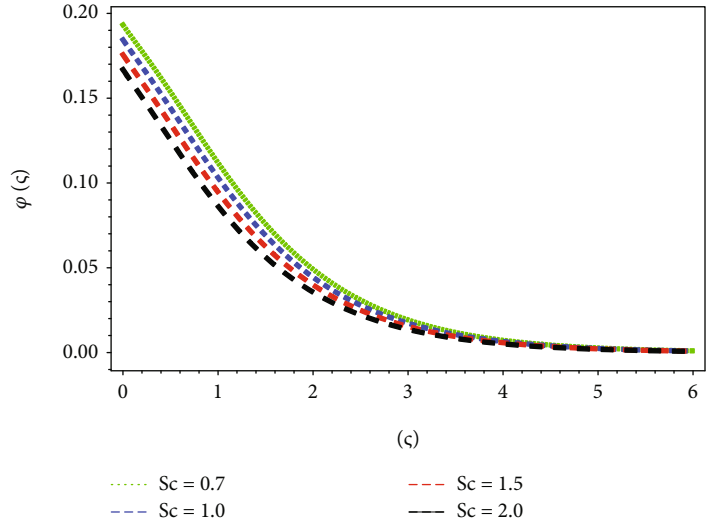

Figure 16: Nanoparticle volume fraction via *Sc*.

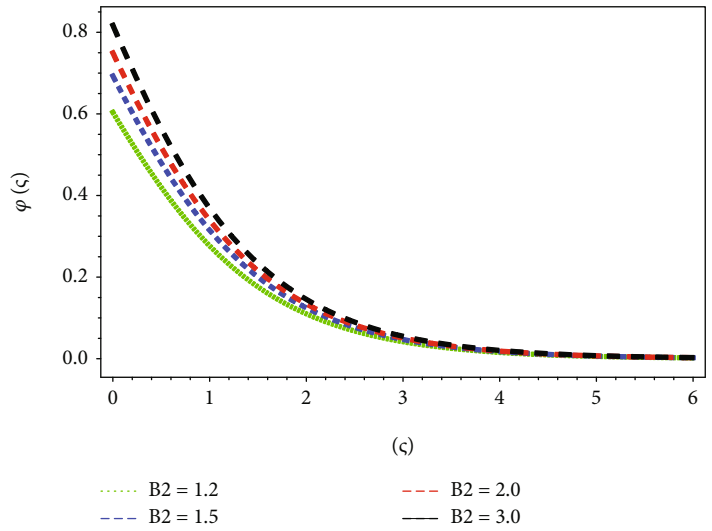

Figure 17: Nanoparticle volume fraction via B_2.

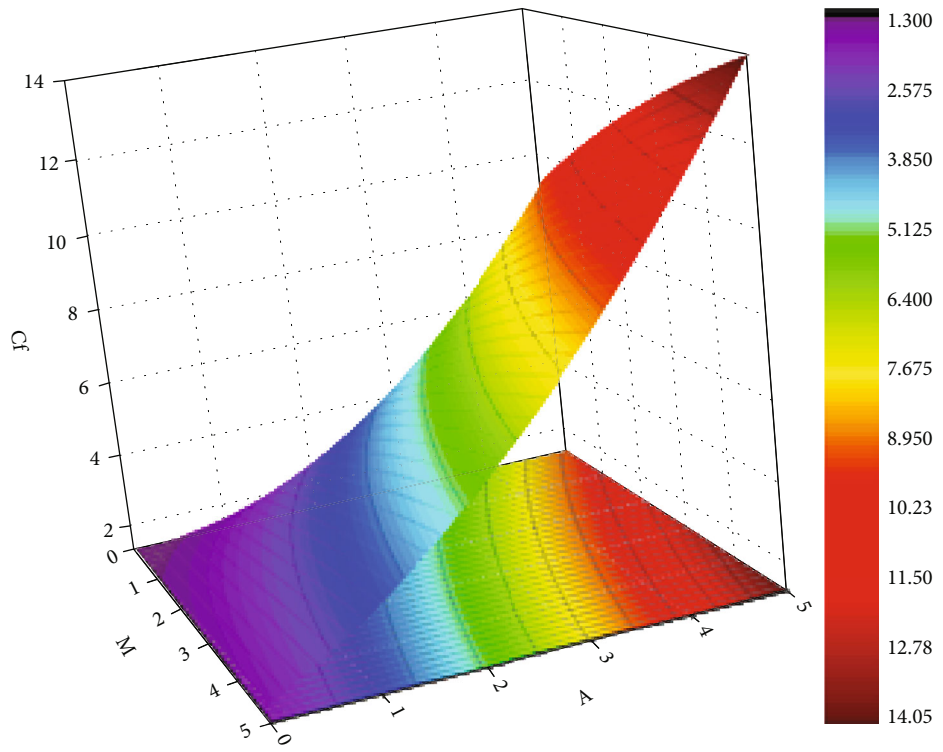

Figure 18: Results of M and A via Cf_x.

Biot number B_1 on $\theta(\varsigma)$ is portrayed in Figure 11. It is cognized that temperature profiles of nanofluid increase with rising values of B_1. Figure 12 explains the effect of heat generation parameter$S$ on $\theta(\varsigma)$ thermal curves. The energy field of the nanofluid increases with larger estimation of S. Physically, upsurging values of S add extra thermal energy to the entire flow domain. Variation in $\theta(\varsigma)$ energy profiles is shown in Figure 13. The thermal field $\theta(\varsigma)$ sketches enhance in the entire flow of nanofluid with increasing data of Ec. Figure 14 discloses the sway of Pr on $\theta(\varsigma)$ sketches of nanofluid. It is noticed that thermal diffusivity decreases with the incrementing values of Pr. Hence, $\theta(\varsigma)$ curves decline.

Figure 15 describes the power of E_1 on $\varphi(\varsigma)$ concentration distribution nanofluids. It is pointed out that $\varphi(\varsigma)$ augmented with upsurging values of E_1. Figure 16 shows the role of Sc on $\varphi(\varsigma)$. The improving values of Sc diminish the concentration profiles. The lower values of Sccorrespond to the uppermost $\varphi(\varsigma)$ of nanoscale materials. In an increment in theSc, there is a decline in the$\varphi(\varsigma)$due to the

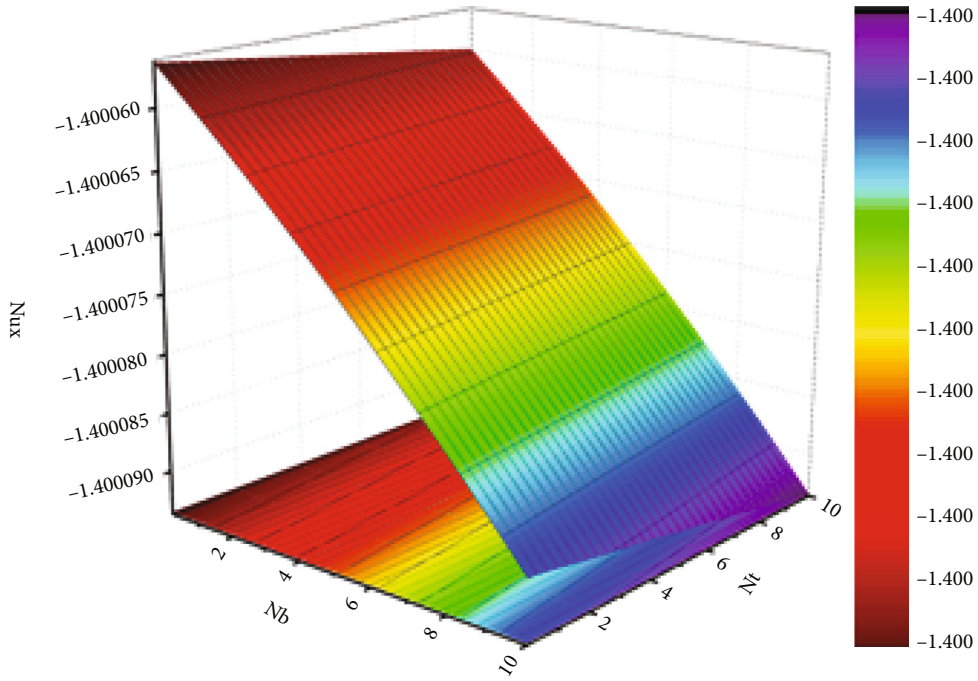

Figure 19: Results of Nb and Nt via Nu_x.

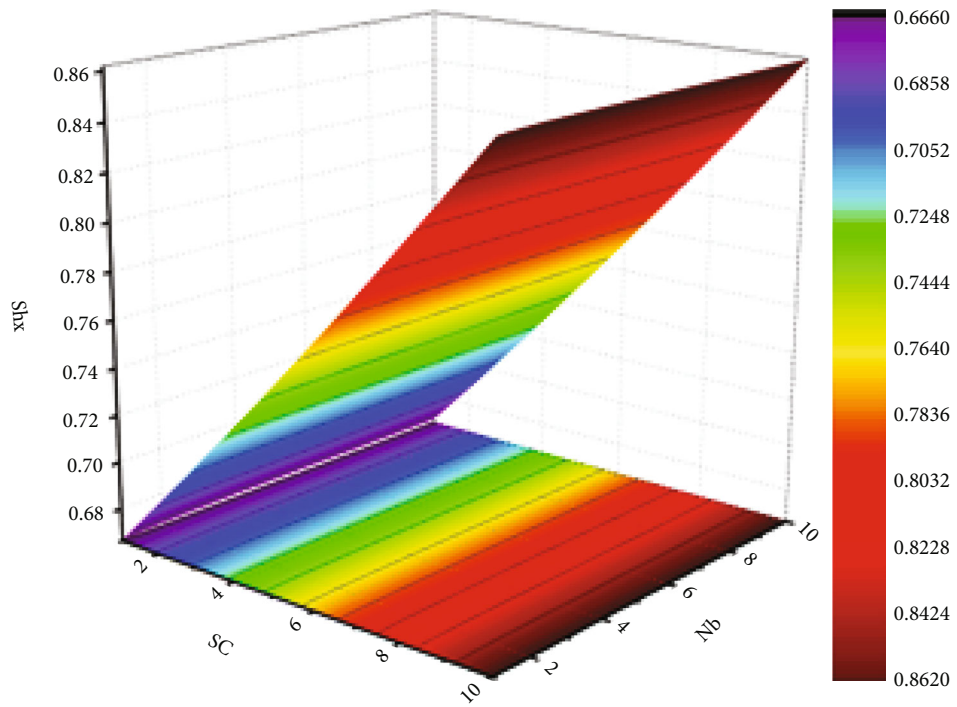

Figure 20: Results of Sc and Nb via Sh_x.

mass diffusion. The impression of B_2 on $\varphi(\varsigma)$ is revealed in Figure 17. The increasing data of B_2 enhances $\varphi(\varsigma)$ profiles. One can observe that $\varphi(\varsigma)$ is the increasing function of B_2. Figure 18 displays the variation of Cf_x for diverse values of M and A. As expected, both parameter the surface drag force with larger estimation of these factors. Figure 19 shows the variation of Nu_x for unlike values of Nb and Nt. It has been detected from this plot that Nu_x gets dwindled for higher values of these parameters. Figure 20 shows the deviation in mass flow rate coefficient Sh_x. As witnessed, mass transfer rate increases for increasing data of Nb and Sc.

5. Conclusions

From this study, the following conclusions can be drawn:

(i) It has been noticed that boundary layers in $F'(\varsigma)$ profiles diminish for incrementing data of M and We, whereas increasing the A, N, and λ caused the $F'(\varsigma)$ profiles to upsurge

(ii) The thermal field curves and heat transfer rates got boost due to augmentation in M, R, S, and Ec along with Nb, Nt, and B_1

(iii) With the upsurge in the Pr, the fluid thermal energy and related thickness dwindle

(iv) The fluid concentration curves increase owing to increase B_2, E_1, and Nt. Moreover, increasing Nb and Sc caused the temperature profiles to diminish

(v) The surface drag force coefficient Cf_x enhances with higher data of M and A parameters

(vi) It has been found that the heat transfer coefficient Nu_x decays via increasing values of Nb and Nt parameters

(vii) Uprising of mass flow rate Sh_x is detected for the increasing values of Sc and Nb parameters

Data Availability

The data used to support the findings of this study are available from the corresponding author upon request.

Conflicts of Interest

The authors declare no conflict of interest.

Acknowledgments

This study was supported by the Princess Nourah bint Abdulrahman University Researchers Supporting Project number (PNURSP2022R184), Princess Nourah bint Abdulrahman University, Riyadh, Saudi Arabia.

References

[1] J. Maxwell, *A Treatise on Electricity and Magnetism*, Oxford University Press, Cambridge, UK, England, 1904.

[2] S. U. S. Choi, Z. G. Zhang, W. Yu, F. E. Lockwood, and E. A. Grulke, "Anomalous thermal conductivity enhancement in nanotube suspensions," *Applied Physics Letters*, vol. 79, no. 14, pp. 2252–2254, 2001.

[3] S. U. S. Choi, "Enhancing thermal conductivity of fluids with nanoparticles," *ASME International Mechanical Engineering Congress & Exposition*, pp. 99–105, 1995.

[4] H. Sadaf and S. I. Abdelsalam, "Adverse effects of a hybrid nanofluid in a wavy non-uniform annulus with convective boundary conditions," *RSC Advances*, vol. 10, no. 26, pp. 15035–15043, 2020.

[5] M. M. Bhatti, R. Ellahi, A. Zeeshan, M. Marin, and S. I. Abdelsalam, "Swimming of motile gyrotactic microorganisms and nanoparticles in blood flow through anisotropically tapered arteries," *Frontiers in Physics*, vol. 8, pp. 1–9, 2020.

[6] S. I. Abdelsalam and M. M. Bhatti, "Anomalous reactivity of thermo-bioconvective nanofluid towards oxytactic microorganisms," *Applied Mathematics and Mechanics*, vol. 41, no. 5, pp. 711–724, 2020.

[7] K. S. Mekheimer, W. M. Hasona, R. E. Abo-Elkhair, and A. Z. Zaher, "Peristaltic blood flow with gold nanoparticles as a third grade nanofluid in catheter: application of cancer therapy," *Physics Letters A*, vol. 382, no. 2-3, pp. 85–93, 2018.

[8] M. Sohail, R. Naz, and S. I. Abdelsalam, "On the onset of entropy generation for a nanofluid with thermal radiation and gyrotactic microorganisms through 3D flows," *Physica Scripta*, vol. 95, no. 4, article 045206, 2020.

[9] S. I. Abdelsalam and M. M. Bhatti, "The study of non-Newtonian nanofluid with hall and ion slip effects on peristaltically induced motion in a non-uniform channel," *RSC Advances*, vol. 8, no. 15, pp. 7904–7915, 2018.

[10] S. I. Abdelsalam and M. M. Bhatti, "The impact of impinging TiO2 nanoparticles in Prandtl nanofluid along with endoscopic and variable magnetic field effects on peristaltic blood flow," *Multidiscipline Modeling in Materials and Structures*, vol. 14, no. 3, pp. 530–548, 2018.

[11] H. Rout, S. S. Mohapatra, S. Shaw, T. Muhammad, M. K. Nayak, and O. D. Makinde, "Entropy optimization for Darcy–Forchheimer electromagneto-hydrodynamic slip flow of ferronanofluid due to stretching/shrinking rotating disk," in *Waves in Random and Complex Media*.

[12] A. Hafeez, M. Khan, and J. Ahmed, "Thermal aspects of chemically reactive Oldroyd-B fluid flow over a rotating disk with Cattaneo–Christov heat flux theory," *Journal of Thermal Analysis and Calorimetry*, vol. 144, no. 3, pp. 793–803, 2021.

[13] M. G. Reddy, N. Kumar, B. C. Prasannakumara, N. G. Rudraswamy, and K. G. Kumar, "Magnetohydrodynamic flow and heat transfer of a hybrid nanofluid over a rotating disk by considering Arrhenius energy," *Communications in Theoretical Physics*, vol. 73, no. 4, p. 045002, 2021.

[14] Y. Kang, C. Yang, and X. Huang, "Electroosmotic flow in a capillary annulus with high zeta potentials," *Journal of Colloid and Interface Science*, vol. 253, no. 2, pp. 285–294, 2002.

[15] S. Ghosal, "Electrokinetic flow and dispersion in capillary electrophoresis," *Annual Review of Fluid Mechanics*, vol. 38, no. 1, pp. 309–338, 2006.

[16] U. Ghosh and S. Chakraborty, "Electroosmosis of viscoelastic fluids over charge modulated surfaces in narrow confinements," *Physics of Fluids*, vol. 27, no. 6, article 062004, 2015.

[17] K. S. Mekheimer, W. M. Hasona, A. A. El-Shekhipy, and A. Z. Zaher, "Electrokinetics of dielectric non-Newtonian bio fluids with heat transfer through a flexible channel: numerical study," *Computational Methods in Science and Technology*, vol. 23, pp. 331–341, 2017.

[18] H. Keramati, A. Sadeghi, M. H. Saidi, and S. Chakraborty, "Analytical solutions for thermo-fluidic transport in electroosmotic flow through rough microtubes," *International Journal of Heat and Mass Transfer*, vol. 92, pp. 244–251, 2016.

[19] A. J. Christopher, N. Magesh, R. J. P. Gowda, R. N. Kumar, and R. S. V. Kumar, "Hybrid nanofluid flow over a stretched cylinder with the impact of homogeneous–heterogeneous reactions and Cattaneo–Christov heat flux: series solution and numerical simulation," *Heat Transfer*, vol. 50, no. 4, pp. 3800–3821, 2021.

[20] R. J. P. Gowda, A. M. Jyothi, R. N. Kumar, B. C. Prasannakumara, and I. E. Sarris, "Convective flow of second grade fluid over a curved stretching sheet with Dufour and Soret effects," *International Journal of Applied and Computational Mathematics*, vol. 7, pp. 1–16, 2021.

[21] A. Alhadhrami, C. Vishalakshi, B. Prasanna et al., "Numerical simulation of local thermal non-equilibrium effects on the flow and heat transfer of non-Newtonian Casson fluid in a porous media," *Case Studies in Thermal Engineering*, vol. 28, p. 101483, 2021.

[22] B. Ali, S. Hussain, M. Shafique, D. Habib, and G. Rasool, "Analyzing the interaction of hybrid base liquid C2H6O2–H2O with hybrid nano-material Ag–MoS2 for unsteady rotational flow referred to an elongated surface using modified Buongiorno's model: FEM simulation," *Mathematics and Computers in Simulation*, vol. 190, pp. 57–74, 2021.

[23] B. Ali, R. A. Naqvi, D. Hussain, O. M. Aldossary, and S. Hussain, "Magnetic rotating flow of a hybrid nanomaterials Ag-MoS2 and Go-MoS2 in C2H6O2-H2O hybrid base fluid over an extending surface involving activation energy: FE simulation," *Mathematics*, vol. 8, no. 10, p. 1730, 2020.

[24] B. Ali, A. Shafiq, I. Siddique, Q. Al-Mdallal, and F. Jarad, "Significance of suction/injection, gravity modulation, thermal radiation, and magnetohydrodynamic on dynamics of micropolar fluid subject to an inclined sheet via finite element approach," *Case Studies in Thermal Engineering*, vol. 28, article ???, 2021.

[25] B. Ali, T. Thumma, D. Habib, N. Salamat, and S. Riaz, "Finite element analysis on transient MHD 3D rotating flow of Maxwell and tangent hyperbolic nanofluid past a bidirectional stretching sheet with Cattaneo Christov heat flux model," *Thermal Science and Engineering Progress*, vol. 28, article 101089, 2022.

[26] B. Ali, I. Siddique, A. Ahmadian, N. Senu, L. Ali, and A. Haider, "Significance of Lorentz and Coriolis forces on dynamics of water based silver tiny particles via finite element simulation," *Ain Shams Engineering Journal*, vol. 13, no. 2, p. 101572, 2022.

[27] M. Buren and Y. Jian, "Electromagnetohydrodynamic (EMHD) flow between two transversely wavy microparallel plates," *Electrophoresis*, vol. 36, no. 14, pp. 1539–1548, 2015.

[28] M. M. Bhatti, A. Zeeshan, N. Ijaz, O. Anwar Bég, and A. Kadir, "Mathematical modelling of nonlinear thermal radiation effects on EMHD peristaltic pumping of viscoelastic dusty fluid through a porous medium duct," *Engineering Science and Technology, an International Journal*, vol. 20, no. 3, pp. 1129–1139, 2017.

[29] R. E. Abo-Elkhair, K. S. Mekheimer, and A. Z. Zaher, "Electromagnetohydrodynamic oscillatory flow of a dielectric fluid through a porous medium with heat transfer: Brinkman model," *Bio Nano Science*, vol. 8, no. 2, pp. 1–13, 2018.

[30] M. I. Khan, "Transportation of hybrid nanoparticles in forced convective Darcy-Forchheimer flow by a rotating disk," *International Communications in Heat and Mass Transfer*, vol. 122, p. 105177, 2021.

[31] T. Hayat, S. Qayyum, M. I. Khan, and A. Alsaedi, "Entropy generation in magnetohydrodynamic radiative flow due to rotating disk in presence of viscous dissipation and Joule heating," *Physics of Fluids*, vol. 30, no. 1, article 017101, 2018.

[32] H. Ur Rasheed, A. AL-Zubaidi, S. Islam, S. Saleem, Z. Khan, and W. Khan, "Effects of joule heating and viscous dissipation on magnetohydrodynamic boundary layer flow of Jeffrey nanofluid over a vertically stretching cylinder," *Coatings*, vol. 11, no. 3, p. 353, 2021.

[33] S. Islam, H. Ur Rasheed, K. S. Nisar, N. A. Alshehri, and M. Zakarya, "Numerical simulation of heat mass transfer effects on MHD flow of Williamson nanofluid by a stretching surface with thermal conductivity and variable thickness," *Coatings*, vol. 11, no. 6, p. 684, 2021.

[34] H. U. Rasheed, S. Islam, Z. Khan et al., "Thermal radiation effects on unsteady stagnation point nanofluid flow in view of convective boundary conditions," *Mathematical Problems in Engineering*, vol. 2021, 13 pages, 2021.

[35] H. U. Rasheed, S. Islam, Z. Khan, S. O. Alharbi, H. Alotaibi, and I. Khan, "Impact of nanofluid flow over an elongated moving surface with a uniform hydromagnetic field and nonlinear heat reservoir," *Complexity*, vol. 2021, Article ID 9951162, 9 pages, 2021.

[36] A. Zaib, K. Bhattacharyya, and S. Shafie, "Unsteady boundary layer flow and heat transfer over an exponentially shrinking sheet with suction in a copper-water nanofluid," *Journal of Central South University*, vol. 22, no. 12, pp. 4856–4863, 2015.

[37] A. K. Pandey, S. Rajput, K. Bhattacharyya, and P. Sibanda, "Impact of metal oxide nanoparticles on unsteady stagnation point flow of the hybrid base fluid along a flat surface," *Pramana*, vol. 95, no. 1, 2021.

[38] S. J. Liao, *Homotopy analysis method in nonlinear differential equations*, Springer & Higher Education Press Heidelberg, Shanghai, China, 2012.

[39] S. Liao, *Beyond Perturbation: Introduction to the Homotopy Analysis Method*, Chapman & Hall/CRC, Boca Raton, 2003.

[40] S. J. Liao, "An optimal homotopy-analysis approach for strongly nonlinear differential equations," *Communications in Nonlinear Science and Numerical Simulation*, vol. 15, no. 8, pp. 2003–2016, 2010.